Deformation of math xmlns="http://www.w3.org/1998/Math/MathML">msub>mi >ZrSiO/mi>mn>4/mn>/msub>/math>-MgO aggregates: Deviatoric stress as a control on deformation mechanisms

Xiaoling Zhou, Lianyang Chen, Mingzhi Yuan, Feng Lin, Tian Ye, Feng Zhao, Martin Kunz, and Lowell Miyagi

Phys. Rev. B **105**, L220101 — Published 3 June 2022

DOI: 10.1103/PhysRevB.105.L220101

Deformation of Zircon + MgO aggregates: Deviatoric Stress as a Control on Deformation Mechanisms

Xiaoling Zhou[1,2,3,4#]*, Lianyang Chen[5#], Mingzhi Yuan[1,6#], Feng Lin[2], Tian Ye[5], Feng Zhao[7,8], Martin Kunz[3], Lowell Miyagi[2]*

[1]School of Science, Harbin Institute of Technology, Shenzhen, Guangdong 510085, China

[2]Department of Geology and Geophysics, University of Utah, Salt Lake City, UT 84112, USA

[3]Advanced Light Source, Lawrence Berkeley National Lab, Berkeley, CA 94720, USA

[4]Department of Geosciences, Princeton University, Princeton, NJ 08542, USA

[5]School of Aeronautics, Northwestern Polytechnical University, Xi'an, Shaanxi 710072, China

[6]Center for High Pressure Science and Technology Advanced Research, Shanghai 201203, China

[7]Institute for Advanced Study, Chengdu University, Chengdu, Sichuan 610106, China

[8]Institute for Advanced Materials Deformation and Damage from Multi-Scale, Chengdu University, Chengdu, Sichuan 610106, China

#These authors contribute equally to this work.

*Corresponding email: zhouxiaoling@hit.edu.cn, lowell.miyagi@utah.edu

Abstract

Deformation behavior of multi-phase aggregates has great significance for materials designs and understanding the dynamics of the Earth. Here we studied deformation of zircon (ZrSiO4)-MgO aggregates and found that the introduction of MgO reduced overall deviatoric stress in the aggregates and thus controlled deformation mechanisms of zircon phase. Zircon primarily deforms by a dominant {101}<10-1> slip; however, activity of zircon {100}<010> slip increases with the introduction of increased ratio of MgO into the aggregates, as suggested by the experiments and simulations. We also found both zircon and MgO in the aggregates remained strong deformation texture, which is likely related to the symmetric variants of dominant slip

system of hard zircon phase. Our results help to clarify the discrepancies in previous studies and understand which phase may dominate the seismic anisotropy in geosciences.

Ⅰ. INTRODUCTION

Deformation behavior of multi-phase aggregates is a fundamental subject for both materials science and Earth sciences. The industrial applications of designed composite materials require the understanding of deformation behavior of multiphase aggregates. In geosciences, it is believed that the seismic anisotropy in the Earth's interior is caused by the texture (lattice preferred orientation) of minerals developed in the deformation process [1-5]. However, most previous deformation studies have focused on single phases [1-5] and studies on multi-phase minerals are less and in demand. In a few high pressure deformation studies on minerals such as bridgmanite + magnesiowüstite aggregates [6,7] and $NaMgF_3$ perovskite + NaCl aggregates [8], researchers have found that soft phases like magnesiowüstite and NaCl do not develop texture and the hard phases like bridgmanite and perovskite develop deformation texture. Instead, deformation on $CaGeO_3$ perovskite + MgO aggregates [9] and NaCl +MgO aggregates [10] indicated that both hard and soft phases developed a texture. It thus brings confusions about which phase would dominate the texture evolution of the whole system and whether the phase symmetry has an effect on the texture of multiphase. These discrepancies indicate that deformation of multi-phase aggregates and the underlying physics warrants further study.

Zircon (ZrSiO$_4$) is a ubiquitous mineral in Earth's crust and a key for geochronology and record for impact events but its deformation behavior remains controversial [11-16]. Different dominant slip systems of zircon including {100}<010> [11,16], {100}<001> [12,13], (001)<100> [13,16], {110}<001> [13] have been proposed. A recent diamond anvil cell (DAC) deformation study [17] on zircon-type $GdVO_4$ suggested that $GdVO_4$ deforms by dominant (001)<100> and

{112}<11-1> slip but it remains unclear whether zircon has the same slip activities. Hence an in-situ deformation study on zircon is expected to resolve the debates on the dominant slip of zircon.

Here we choose pure zircon and zircon-MgO aggregates to study the slip systems of zircon and deformation behavior of multiphase aggregates at high pressure. Zircon + MgO aggregates represent a combination of tetragonal + cubic symmetries that has not been explored in previous deformation studies. Additionally, MgO is a common refractory material in industries and the second most abundant material in the Earth's lower mantle [18]. At room temperature MgO deforms primarily by {110}<1-10> slip [19]. The good stability of MgO and the relatively simple structures and symmetries of zircon and MgO make them good candidate minerals for this multi-phase deformation study. By conducting diamond anvil cell (DAC) combined with synchrotron radial X-ray diffraction (XRD) experiments, Elasto–ViscoPlastic Self-Consistent (EVPSC) [20] simulations and transmission electron microscopy (TEM) characterization, we investigated the deformation slips of zircon and the texture evolutions in a single and multi-aggregates system. We show a new dominant slip of zircon which has not been reported before and reveal the correlations between the phase friction of MgO and deformation mechanisms of zircon. We also discussed how the dominant slip system of one phase influenced the texture evolutions of another phase in a multi-aggregates system.

Ⅱ. METHODS

Ground pure zircon powder sample and zircon-MgO mixtures were pre-compacted and loaded into boron-kapton gaskets mounted in a DAC with 300 μm culet anvils, respectively. Pt and MgO were used as pressure calibrants for pure zircon and zircon-MgO mixture deformation experiments, respectively. No pressure medium was used to maximize the differential stress in the chamber. High pressure synchrotron XRD measurements in radial geometry were performed at Beamline 12.2.2 of the Advanced Light Source (ALS), Lawrence Berkeley National Laboratory, USA. A monochromatic beam with an energy of 25 keV and 30 keV were used for the deformation experiments of pure zircon and zircon+MgO mixtures, respectively. The diffraction pattern was refined with the Rietveld method using the Materials Analysis Using Diffraction (MAUD) software [21]. More details could be found in Supplementary Materials [22-26]. The volume ratio of MgO was obtained from the XRD refinements.

The EVPSC code [20] is used to model our experimental data and twelve possible systems including {100}<010>, {100}<001>, {100}<011>, (001)<110>, (001)<100>, {101}<10-1>, {112}<11-1>, {112}<110>, {111}<1-10>,{110}<001> slips and {112}<11-1> twinning and {101}<10-1> twinning have been considered in the simulation. Due to the potential effects of the reidite transformation on texture and Q(hkl) evolution we only run simulations for P<25 GPa to minimize the effects of the phase transition. Parameters including the strain, compression rate (strain rate) and critical resolved shear stress (CRSS) values of possible slip systems and twin modes are adjusted to reproduce the experimental lattice strain and texture evolution as function of pressure. More simulation details could be found in Supplementary Materials [22].

Ground pure zircon and the zircon-MgO mixture powder samples were pre-compacted and loaded into steel gaskets mounted in a DAC with 300 μm culet anvils, respectively. Ruby was used as the pressure calibrant and the highest pressure was increased to ~ 30 GPa to minimize the effects of the phase transition. The post-deformed samples were thinned by focused ion beam (FIB) and prepared for TEM characterization. The energy dispersive spectra (EDS) indicate that the volume ratio of MgO is around 48% in the zircon-MgO mixture. Bright field imaging (BF) and selected area diffraction (SAD) were performed on both pure sample and zircon-48%MgO mixture by using a FEI Talos F200X TEM operating at 200 kV. BF and SAD were utilized to examine the dislocation with different slip systems. More analysis could be found in Supplementary Materials [22,27].

Ⅲ. RESULTS AND DISCUSSIONS

We observed the zircon ($I4_1/amd$)- reidite ($I4_1/a$) phase transition starting around 20 GPa (Fig. S1), which was consistent with previous studies [28-30]. Deviatoric lattice strain *Q*(hkl) and differential/deviatoric stress *t*(hkl) of each lattice plane of zircon phase were obtained and calculated. As shown in Fig. 1(a), the (220) planes and (200) planes exhibit the highest and lowest flow strength among the four measured lattice planes in pure zircon. With an increased volume ratio of MgO added to the mixture (Fig. 1(b-c)), the strength order of the different planes of zircon changes. Specifically, in the 40% MgO sample *t*(220) of zircon decreases to a similar level as *t*(211) (Fig. 1(c)). The overall stress levels decrease significantly with stresses in the pure zircon sample being ~ twice as large as in zircon that is mixed with 40% MgO. The order of *Q*(hkl) and *t*(hkl) is directly related to the activity of deformation mechanisms (twinning and dislocations glide). Thus, this change in *t*(hkl) order and relative magnitude may be related to changes in dislocation or twin activity in the zircon phase.

We analyzed the texture evolution of zircon in the pure and mixed samples during compression (Fig. 1(d)). As shown in the inverse pole figures (IPFs), in pure zircon a (001) maxima develops at ~10 GPa and continues to strengthen during further compression (Fig. 1d). In the zircon-25% MgO mixture, zircon first develops a weak (110) maxima that is then overprinted by a (001) texture around ~ 13 GPa. In the zircon-40% MgO mixture, zircon initially develops a stronger (110) maxima than the 25% sample, and this is gradually overprinted by an (001) deformation texture. In the 40% MgO sample zircon does not fully develop a (001) texture until ~38 GPa. Furthermore the texture strength of zircon is considerably lower in the 40% MgO sample than in the pure zircon sample. The fact that the initial (110) texture becomes more pronounced with higher volume fractions of MgO suggests that the addition of a secondary phase has a significant effect on the development of deformation textures in the zircon phase.

The deformation texture change from (110) to (001) suggests a change in deformation mechanism of zircon. We use the EVPSC method [20] which has been modified for high pressure deformation [31] to simulate the *Q*(hkl) values and deformation textures of zircon with a range of possible slip and twinning systems including {100}<010> [11,16], {100}<001> [12,13], (001)<100> [13,16], {110}<001> [13] slip systems (see Supplementary Materials [22]). We also include slip on {112}<11-1> as has been suggested for zircon structured $GdVO_4$ [17] and slip on {101}<10-1> which is common in a wide range of tetragonal materials [32-35] and has been proposed for high pressure deformation of stishovite [36]. We tried combinations of these possible slip systems to finely tune the match to experimental textures and *Q*(hkl) values for pure zircon and zircon mixed with MgO. As shown in Fig. 2(a-c), the simulated *Q*(hkl) values agree well with the experimental results. The simulated textures reproduce an intense (001) maxima observed in pure zircon and zircon mixed with MgO (Fig. 2(d-f)). For pure zircon, zircon-25% MgO and zircon-40% MgO, the simulated maximum texture magnitude is 3.5 m.r.d. (at a 21% strain, ~24 GPa), 3.0 m.r.d. (at a 20% strain, ~25 GPa), 2.4 m.r.d (at a 17.5% strain, ~ 25 GPa), respectively, which are comparable to the fitted value of 4.4. m.r.d. (at 24 GPa), 3.4 m.r.d (at 25 GPa), 2.6 m.r.d (at 26 GPa) obtained from the experiments. We also note that the simulated texture evolution does not fully reproduce the (110) maxima that is observed in the experimental data for the 40% MgO sample and to a lesser extent the 25% MgO sample (Fig. 1(d)). This may be due to the fact that EVPSC and self-consistent simulations in general do not account for the effects of microstructure on texture and lattice strain evolution. Zircon is well known to cleave on {110} and it is likely that grinding results in platy grains that are flattened on {110}. In the 40% MgO sample when zircon grains are fully surrounded by the softer MgO phase, rigid grain rotation may occur resulting in the alignment of zircon grains with {110} cleavage planes at high angles to compression. As we do not account for crystallographically flattened grains in our simulations this may be why we fail to reproduce the initial development of a (110) maxima in the experimental IPFs. The EVPSC simulations suggest the dominant {101}<10-1> slip to be most consistent with the experimental results (Fig. 2(g-i)). With the increased volume ratio of MgO, the minor activity of (001)<100> and {100}<001> slip systems weaken while the activity of {100}<010> slip remarkably increases.

To reveal the physics behind we performed the TEM characterization on the post-deformed samples recovered from high pressure experiments. As shown in Fig. 3(a), high densities of dislocation lines perpendicular to the <10-1> direction indexed by the SAD pattern were observed in the pure sample, suggesting that the {101}<10-1> slip could be dominant. Remarkably, in the mixed sample another set of dislocations were also found to intersect with the {101}<10-1> slip with an angle of ~ 60° (Fig. 3(b)), which is corresponding to the intersection angle between {101}<10-1> and {100}<010> slips when projected on the (111) plane. Hence, the second set of dislocations were associated with the {100}<010> slip (see Supplementary Materials [22] and Fig. S3) and there were increased densities of {100}<010> slips observed in the mixed sample (Fig. 3(b)). These observations strongly support our results from the EVPSC simulations and XRD experiments that {101}<10-1> is the dominant slip in zircon whereas the activity of {100}<010> slip increases with the introduction of MgO into zircon sample. It is worth noting that deformation bands were also observed in the TEM images, which indicated the severe and heterogeneous deformation of the samples subjected to the large shear stress.

The origin of different deformation pathways in zircon should be the deviatoric stress influenced by the introduction of softer MgO phase. As shown in Fig. 1(a-c), before structural transition (< 20 GPa) the average differential / deviatoric stress of zircon gradually decreases with the increase of MgO and *t*(220) becomes comparable to *t*(211) in zircon mixed with 40% of MgO. This suggests that the overall shear stress imposed on zircon decreases and the stress field in zircon redistributes because of the introduction of softer MgO phase. The change in stress field may result in the modification of atomic densities in crystallographic planes. Generally the crystallographic plane with a larger *d*-spacing exhibits a higher atomic density and is more energetically favorable when the slip occurs. In this case the *d*-spacing of (100) plane is larger than the (101) plane (Fig. S4), indicating that the slip on (100) plane is more energetically favorable at low deviatoric stress. Meanwhile, the differences in *d*-spacing between the (100) and (101) plane are systematically larger in zircon mixed with MgO than that of pure sample (Fig. S4), suggesting that the atomic density of (100) plane is relatively increased comparing to (101) plane and thus the (100) slip is more favorable in the mixed sample than that in pure sample.

Interestingly dislocations with <10-1> burgers vectors are found in our experiments though it is not energetically favorable and have not been observed in previous studies on zircon. Slip on {101}<10-1> is common in tetragonal ceramics [32-35] and is suggested for high pressure deformation of stishovite [36]. We think that high deviatoric stress levels and low temperatures in our experiments favor the activation of the {101}<10-1> slip system in zircon. The high deviatoric stress in our experiments causes the dominant {101}<10-1> slip while the introduction of softer MgO reduces the shear stress on zircon and allows the activation of the {100}<010> system which is generally energetically favorable at low deviatoric stress. In a TEM study on natural zircon samples [37], higher stress conditions tended to result in activation of higher order slip systems while in contrast zircon grains contained in a softer matrix tended to only deform by energetically favorable slip systems such as {100}<010>. This is consistent with our results that the {100}<010> slip system is energetically favorable at low deviatoric stress and the deviatoric stress controls the deformation mechanisms of zircon though the dominant {101}<10-1> slip system has not been reported before.

Our analysis shows distinct results from previous experimental studies on slip systems of zircon. In natural zircon samples, compositional variation or chemical environment change might be the cause for different slip system activities. Zircon deformed by tectonic events or shock compression experiences distinctly different strain rate and high temperature processing comparing with static DAC compression. Studies on olivine suggested that factors such as strain rate, temperature, pressure, deviatoric stress, and chemical conditions including water and oxygen fugacity, would play roles in changing the slip system and texture type of olivine [1,4,38]. In this scenario, either change in composition or chemical environment in natural samples or change in strain rate and temperature in previous tectonic events or shock experiments could lead to different slip systems of zircon. Our DAC experiments suggest a new dominant {101}<10-1> slip system in zircon, and provide evidence that the deviatoric stress variation controlled by physically tuning phase friction of aggregates could result in different slip activities of zircon. This helps to understand the discrepancies in deformation mechanisms of natural zircon samples or zircon deformed by tectonic events, shock compression and DAC. It also suggests the differences in slip activities and deformation behavior of the same phase in a single and multi-aggregates system. Since the Earth's rocks are natural multi-aggregates systems, deformation experiments and modeling on multi-aggregates system should take the place of single minerals in the future.

We also compared the texture evolution of reidite and MgO in the pure sample and mixed samples across the phase transition (Fig. 4). Reidite in both pure phase and mixtures shows a strong (110) transformation texture inherited from the (001) maxima in zircon. It can be seen that MgO mixed with 75% zircon and 60% zircon both develop a (100) deformation texture (Fig. 4). This is in contrast to previous studies in which the soft magnesiowüstite and NaCl phases remain random [6,8]. Our result is more similar to the texture evolution in the $CaGeO_3$ + MgO and NaCl+MgO deformation studies where both phases develop texture [9,10].

Previous studies documenting texture disruption in the soft phase either contain hard phases that remain undeformed [39-41] or hard phases with low symmetry and a dominant slip system with few or no symmetric variants [7,8]. Numerical simulations and microstructure observations show heterogeneous strain fields within the soft phase which results in a lack of texture development [8,39]. In our case, zircon has the highest differential stress (Fig. S1) and is much harder than MgO. We summarized the dominant slips and their symmetric variants of hard phases from previous studies in Table 1. It is likely that when the hard phase has a dominant slip with few symmetric variants, it imposes more strain heterogeneity and tends to disrupt the texture in the soft phase. Instead a hard phase with dominant slip systems that have many symmetric variants does not impose much strain heterogeneity in the soft phase so the texture of the soft phase preserves. In our study, zircon has a dominant {101}<10-1> slip system with four symmetric variants, which might be the reason for the preservation of texture in the soft MgO phase. This is also evidenced by previous studies [9,10] in which both $CaGeO_3$ and MgO have dominant slips with six symmetric variants and the soft phase develops texture. Further studies are required to check the assumption. Our results show the correlations between slip system and texture evolutions of hard and soft phase in multi-aggregates system. It helps to understand the texture evolutions of minerals in multi-aggregates system and figure out the phase accounting for the seismic anisotropy.

IV. CONCLUSIONS

In summary, our study suggests that the introduction of MgO decreases the deviatoric stress in zircon and controls its deformation mechanisms. EVPSC simulations and TEM characterization indicate that zircon deforms by a dominant {101}<10-1> slip but the activity of zircon {100}<010> slip increases with the introduction of an increased ratio of MgO, suggesting a stress-sensitive deformation pathways of zircon controlled by the second phase. We also found that MgO phase in the aggregates develops a strong (100) deformation texture in contrast to previous studies on orthorhombic + cubic aggregates in which the MgO phase tends to have a random orientation distribution. This is likely related to the symmetric variants of dominant slip system of hard phase and the degree of strain heterogeneity that the hard phase imposes in the softer phase. Our results provide new insights into understanding the role of deviatoric stress levels in controlling zircon deformation pathways especially understanding the discrepancies in previous deformation studies. It also implies that through the introduction of a secondary phase one could adjust the deviatoric stress and control the deformation mechanisms of targeted materials.

ACKNOWLEDGMENTS

The authors thank Prof. Shiteng Zhao for helpful discussions. L. M. acknowledges support from CDAC and NSF EAR-1654687. X. Z. acknowledges the support of ALS Collaborative Postdoctoral Fellowship Program. X. Z. acknowledges the support of National Science Foundation grant EAR-1722495. The Advanced Light Source is supported by the Director, Office of Science, Office of Basic Energy Sciences, Materials Sciences Division, of the U.S. Department of Energy under Contract No. DE-AC02-05CH11231 at Lawrence Berkeley National Laboratory and University of California, Berkeley, California.

References

[1] H. Jung and S.-i. Karato, Science **293**, 1460 (2001).

[2] S. Merkel, A. Kubo, L. Miyagi, S. Speziale, T. S. Duffy, H. K. Mao, and H. R. Wenk, Science **311**, 644 (2006).

[3] S. Merkel, A. K. McNamara, A. Kubo, S. Speziale, L. Miyagi, Y. Meng, T. S. Duffy, and H. R. Wenk, Science **316**, 1729 (2007).

[4] H. Jung, W. Mo, and H. W. Green, Nature Geoscience **2**, 73 (2008).

[5] L. Miyagi, W. Kanitpanyacharoen, P. Kaercher, K. K. Lee, and H. R. Wenk, Science **329**, 1639 (2010).

[6] J. Girard, G. Amulele, R. Farla, A. Mohiuddin, and S.-i. Karato, Science **351**, 144 (2016).

[7] L. Miyagi and H.-R. Wenk, Physics and Chemistry of Minerals **43**, 597 (2016).

[8] P. Kaercher, L. Miyagi, W. Kanitpanyacharoen, E. Zepeda-Alarcon, Y. Wang, D. Parkinson, R. Lebensohn, F. De Carlo, and H. Wenk, Earth and Planetary Science Letters **456**, 134 (2016).

[9] Y. Wang, N. Hilairet, N. Nishiyama, N. Yahata, T. Tsuchiya, G. Morard, and G. Fiquet, Geochemistry, Geophysics, Geosystems **14**, 3389 (2013).

[10] F. Lin, M. Giannetta, M. Jugle, S. Couper, B. Dunleavy, and L. Miyagi, Minerals **9**, 679 (2019).

[11] H. Leroux, W. Reimold, C. Koeberl, U. Hornemann, and J.-C. Doukhan, Earth and Planetary Science Letters **169**, 291 (1999).

[12] S. M. Reddy, N. E. Timms, W. Pantleon, and P. Trimby, Contributions to Mineralogy and Petrology **153**, 625 (2007).

[13] M.-A. Kaczmarek, S. Reddy, and N. E. Timms, Lithos **127**, 414 (2011).

[14] D. Moser, C. Cupelli, I. Barker, R. Flowers, J. Bowman, J. Wooden, and J. Hart, Canadian Journal of Earth Sciences **48**, 117 (2011).

[15] I. Morozova, S. R. Shieh, D. E. Moser, I. R. Barker, and J. M. Hanchar, Microstructural Geochronology: Planetary Records Down to Atom Scale, 167 (2018).

[16] N. E. Timms, D. Healy, T. M. Erickson, A. A. Nemchin, M. A. Pearce, and A. J. Cavosie, Microstructural Geochronology: Planetary Records Down to Atom Scale, 183 (2018).

[17] B. Yue, F. Hong, S. Merkel, D. Tan, J. Yan, B. Chen, and H.-K. Mao, Physical review letters **117**, 135701 (2016).

[18] X. Li, Y. Yuan, J. Zhang, T. Kim, D. Zhang, K. Yang, Y. Lee, and L. Wang, Journal of Physics: Condensed Matter **30**, 194002 (2018).

[19] S. Merkel, H. R. Wenk, J. Shu, G. Shen, P. Gillet, H.-k. Mao, and R. J. Hemley, Journal of Geophysical Research: Solid Earth **107**, ECV 3 (2002).

[20] H. Wang, P. Wu, C. Tomé, and Y. Huang, Journal of the Mechanics and Physics of Solids **58**, 594 (2010).

[21] L. Lutterotti, R. Vasin, and H.-R. Wenk, Powder Diffraction **29**, 76 (2014).

[22] See Supplemental Material at [URL] for Methods and supplementary figures and table.

[23] A. K. Singh, C. Balasingh, H.-k. Mao, R. J. Hemley, and J. Shu, Journal of Applied Physics **83**, 7567 (1998).

[24] H. Özkan and J. Jamieson, Physics and Chemistry of Minerals **2**, 215 (1978).

[25] R. Dutta and N. Mandal, Materials Chemistry and Physics **135**, 322 (2012).

[26] H.-R. Wenk, L. Lutterotti, P. Kaercher, W. Kanitpanyacharoen, L. Miyagi, and R. Vasin, Powder Diffraction **29**, 220 (2014).

[27] C. Y. Wang, C. M. Cepeda-Jiménez, and M. T. Pérez-Prado, Acta Materialia **194**, 190 (2020).

[28] R. M. Hazen and L. W. Finger, American Mineralogist **64**, 196 (1979).

[29] M. Marqués, J. Contreras-García, M. Florez, and J. Recio, Journal of Physics and Chemistry of Solids **69**, 2277 (2008).

[30] K. Kusaba, T. Yagi, M. Kikuchi, and Y. Syono, Journal of Physics and Chemistry of Solids **47**, 675 (1986).

[31] F. Lin, N. Hilairet, P. Raterron, A. Addad, J. Immoor, H. Marquardt, C. Tomé, L. Miyagi, and S. Merkel, Journal of Applied Physics **122**, 205902 (2017).

[32] M. Leoni, J. Martinez-Garcia, and P. Scardi, Journal of Applied Crystallography **40**, 719 (2007).

[33] X. Tan and J. K. Shang, Journal of Physics: Condensed Matter **16**, 1455 (2004).

[34] M. Blanchin, L. Bursill, and C. Lafage, Proceedings of the Royal Society of London. A. Mathematical and Physical Sciences **429**, 175 (1990).

[35] K. Ashbee and R. Smallman, Journal of the American Ceramic Society **46**, 211 (1963).

[36] P. M. Kaercher, E. Zepeda-Alarcon, V. B. Prakapenka, W. Kanitpanyacharoen, J. S. Smith, S. Sinogeikin, and H.-R. Wenk, Physics and Chemistry of Minerals **42**, 275 (2015).

[37] E. Kovaleva, U. Klötzli, G. Habler, and J. Wheeler, American Mineralogist **100**, 1834 (2015).

[38] S.-i. Karato, H. Jung, I. Katayama, and P. Skemer, Annu. Rev. Earth Planet. Sci. **36**, 59 (2008).

[39] G. Canova, H. Wenk, and A. Molinari, Acta metallurgica et materialia **40**, 1519 (1992).

[40] A. Poudens, B. Bacroix, and T. Bretheau, Materials Science and Engineering: A **196**, 219 (1995).

[41] G. Garcés, M. Rodríguez, P. Perez, and P. Adeva, Materials Science and Engineering: A **419**, 357 (2006).

Figure and Table captions:

FIG. 1. (a), (b), and (c), measured mechanical anisotropy change in zircon phase with the introduction of different volume ratios of MgO phase. (d) Measured deformation texture evolution in zircon phase with the introduction of MgO phase at different pressures. The numbers in the left side are pressure in units of GPa.

FIG. 2. EVPSC simulation results for *Q*(hkl) values, texture and slip activities of the zircon phase: (a) (d)(g)pure zircon, (b) (e)(h)25% MgO-zircon and (c)(f)(i) 40%MgO-zircon. The simulated texture is intense in the 001 corner. The maximum texture magnitude is 3.5 m.r.d. for pure zircon at 21% strain (~24 GPa), 3.0 m.r.d. for zircon mixed with 25% MgO at 20% strain (~25 GPa) and 2.4 m.r.d. for zircon mixed with 40% MgO at 17.5% strain (~ 24 GPa). The parameters used in the EVPSC simulation are listed in Table S1.

FIG. 3. TEM observations on the microstructures of post-deformed pure sample (a) and the zircon-MgO mixture (b). The insets are the corresponding SAD patterns viewed from the <111> direction. The red and yellow arrow indicate the {101}<10-1> and {100}<010> dislocation, respectively. The lines are guides for eyes.

FIG. 4. Texture evolutions of zircon, reidite and MgO with increased pressure. The IPFs of reidite phase is asymmetric so that a sector of 90 degree is used.

Table 1. The correlations between dominant slip of hard phase and the texture evolution of soft phase. Phase friction of the soft phase is below 50%.

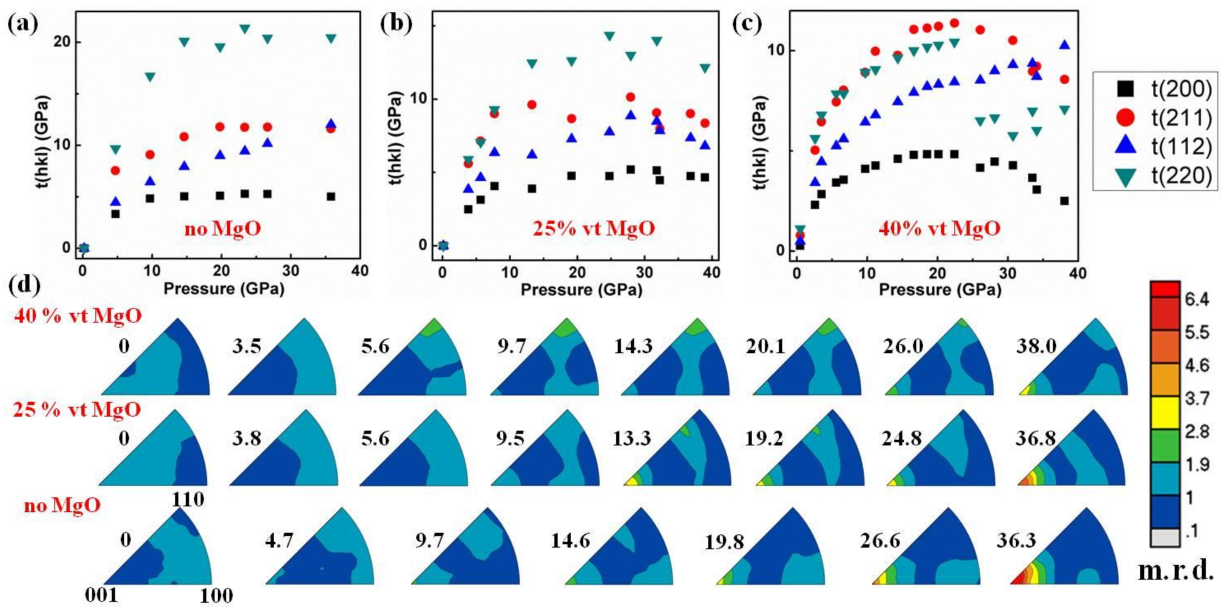
(a)
(b)
(c)
(d)
t(hkl) (GPa)
Pressure (GPa)
no MgO
25% vt MgO
40% vt MgO
t(200)
t(211)
t(112)
t(220)
40 % vt MgO
25 % vt MgO
no MgO
110
001
100
m.r.d.

Figure 1

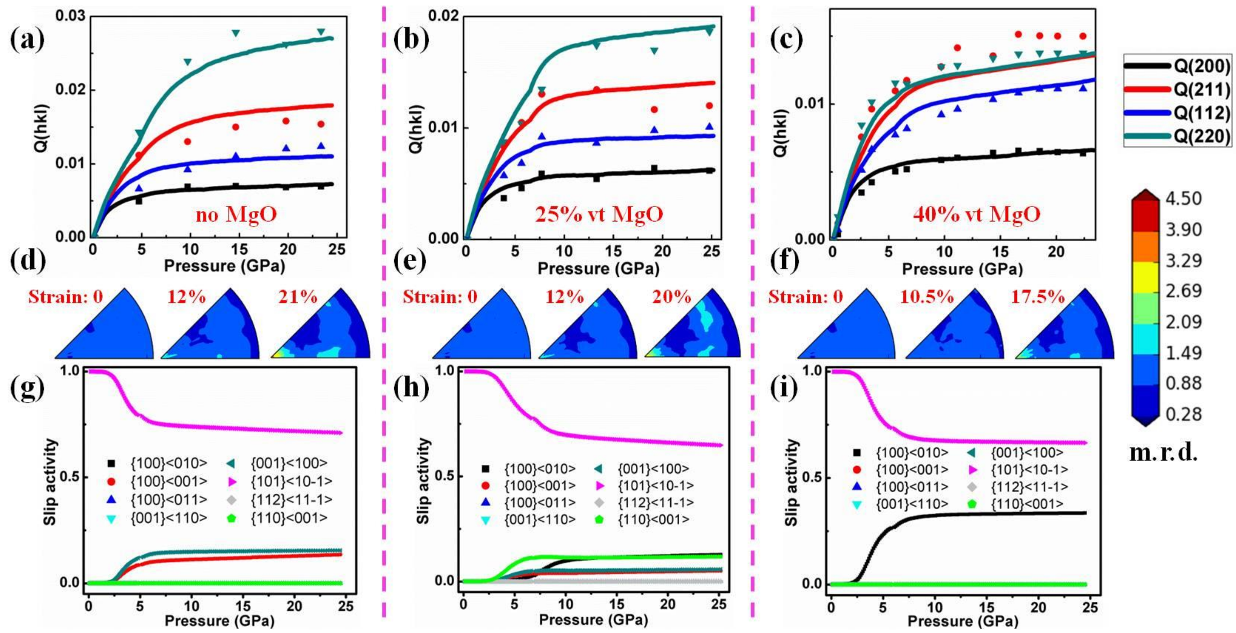
(a)
(b)
(c)
Q(hkl)
Pressure (GPa)
no MgO
25% vt MgO
40% vt MgO
Q(200)
Q(211)
Q(112)
Q(220)
(d)
(e)
(f)
Strain: 0
12%
21%
Strain: 0
12%
20%
Strain: 0
10.5%
17.5%
4.50
3.90
3.29
2.69
2.09
1.49
0.88
0.28
m.r.d.
(g)
(h)
(i)
Slip activity
{100}<010>
{100}<001>
{100}<011>
{001}<110>
{001}<100>
{101}<10-1>
{112}<11-1>
{110}<001>

Figure 2

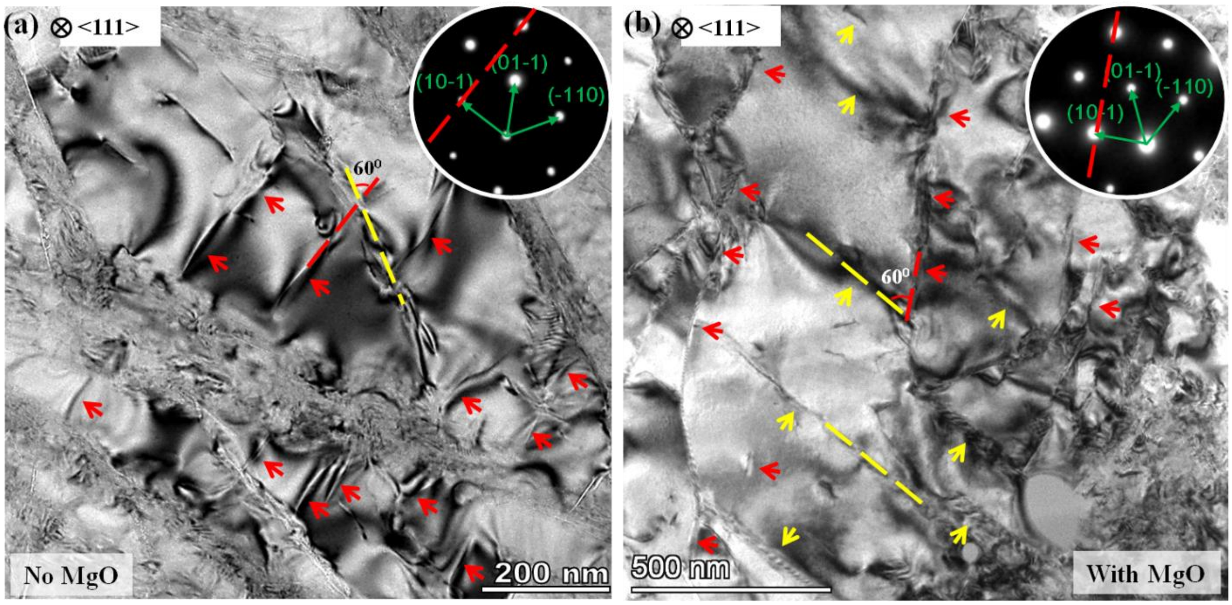
(a) ⊗<111>
(10-1)
(01-1)
(-110)
60°
No MgO
200 nm
(b) ⊗<111>
(01-1)
(-110)
(10-1)
60°
500 nm
With MgO

Figure 3

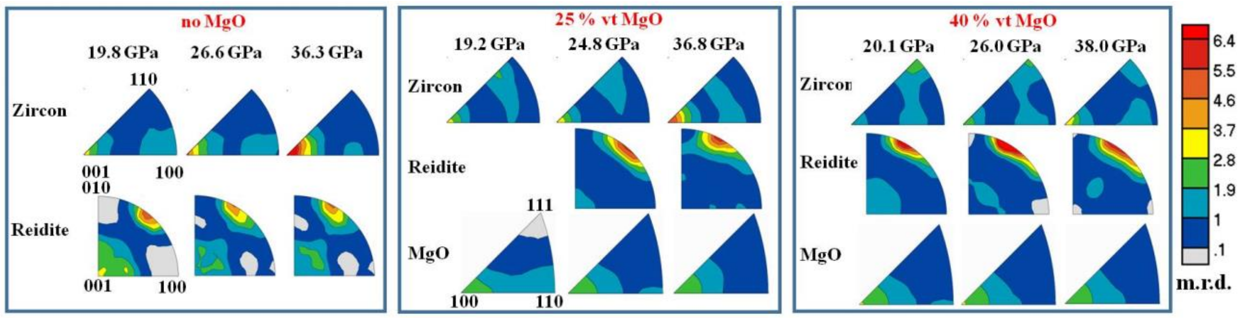
no MgO
19.8 GPa
26.6 GPa
36.3 GPa
Zircon
110
001
100
010
Reidite
001
100
25 % vt MgO
19.2 GPa
24.8 GPa
36.8 GPa
Zircon
Reidite
111
MgO
100
110
40 % vt MgO
20.1 GPa
26.0 GPa
38.0 GPa
Zircon
Reidite
MgO
6.4
5.5
4.6
3.7
2.8
1.9
1
.1
m.r.d.

Figure 4

Hard phase (+ soft phase)	Dominant slip of hard phase	symmetric variants	Soft phase	Reference
$CaGeO_3$ (+MgO)	{110}<1-10>	6	Texture	Ref. [9]
MgO (+NaCl)	{110}<1-10>	6	Texture	Ref. [10]
Zircon (+MgO)	{101}<10-1>	4	Texture	This study
$(Mg,Fe)SiO_3$ (bridgmanite) (+ (Mg,Fe)O)	(100)[010]	1	No texture	Ref. [7]
$NaMgF_3$ (perovskite) (+ NaCl)	(100)[010]	1	No texture	Ref. [8]

Table 1